Available online at www.sciencedirect.com

ScienceDirect

Procedia CIRP 102 (2021) 228–233

www.elsevier.com/locate/procedia

18th CIRP Conference on Modeling of Machining Operations

Surface finish of additively manufactured Ti6Al4V workpieces after ball end milling

Lucia Lizzul[a]*, Marco Sorgato[a], Rachele Bertolini[a], Andrea Ghiotti[a], Stefania Bruschi[a]

[a]*Department of Industrial Engineering, University of Padova, Via Venezia 1, 35131, Padova, Italy*

* Corresponding author. Tel.: +39 49-827 6819. *E-mail address:* lucia.lizzul@phd.unipd.it

Abstract

This work investigates the machinability characteristics of additively manufactured Ti6Al4V titanium alloy workpieces in finishing machining using ball end mills on 45° inclined surfaces. The surface finish results were compared with the ones from ball end milling trials on wrought Ti6Al4V samples using the same cutting conditions. Optical profilometry and scanning electron microscope imaging were used to compare the different surface texture and quality of the two alloys, as well as the chip morphology, with the aim of finding a correlation between the surface finish obtained at varying cutting parameters and the Ti6Al4V peculiar microstructure induced by the additive manufacturing process. The results showed that the additively manufactured alloy allowed for a better surface quality respect to the wrought one. This was attributed to the interactions of the ball mill cutting edge with the α phase colonies of such alloy, which may favor the material removal by locally lowering the material resistance to cutting.

Keywords: Titanium; Additive manufacturing; Ball end milling; Surface finish

1. Introduction

Additive Manufacturing (AM) can be successfully exploited for fabricating parts made of difficult-to-cut metals, such as titanium alloys, nickel superalloys, and stainless steels. In fact, AM allows saving costs, shortening lead times, and reducing material wastage to fabricate free form components that would be difficult to manufacture with conventional processes [1]. Despite the numerous advantages of AM, surface finish of the fabricated part remains one of the major concerns [2]. The automotive and aerospace industries, which can benefit a lot from AM technologies, require, at the same time, high precision and high surface quality. This can be achieved through ball end milling on CNC machining centers. Thanks to this post-processing operation, optimal surface finishing can be attained on complex parts. Despite the great advantages of ball end milling, the literature studies dealing with this machining operation performed on additively manufactured (AMed) metals lack. Some studies were carried out on ball end milling of difficult-to-cut alloys, such as titanium alloys [3,4] and Inconel [5], in terms of surface integrity and surface roughness after machining. However, the studies are limited to conventionally manufactured alloys and no documents were found on AMed alloys. The urge to study the AMed alloys machinability derives from their different microstructure compared to that of conventionally manufactured alloys. In fact, AMed alloys present a high degree of anisotropy in microstructure induced by the fabrication process itself, which is characterized by highly localized heat input with short interaction times, causing high thermal gradients [6]. As a result, the solidification structures are directed along the greater heat flow, which is mostly the build-up direction, leading to an anisotropic microstructure. This reflects on the mechanical properties [7,8], and thus, on the machinability of AMed workpieces [9,10]. In this work, the behavior of 45° inclined Ti6Al4V titanium alloy samples manufactured via Laser

10.1016/j.procir.2021.09.039

Powder Bed Fusion (LPBF) and ball end milled at different cutting parameters was investigated in terms of surface topography, surface defects, and chip morphology. For the sake of comparison, similar analyses were carried out on the same alloy, but conventionally manufactured and then machined through ball end milling. The results of this study are useful for more in-depth understanding of the machinability of AMed alloys since the observed behavior was closely correlated to the microstructural features typical for such alloys.

2. Materials and methods

2.1. Materials

Two kinds of Ti6Al4V grade 5 were investigated in this work: one was additively manufactured via LPBF, here referred to as AM workpiece, and the other was conventionally manufactured, here referred to as WR workpiece. The first one was fabricated using a MYSINT100 SISMA™ machine under argon atmosphere. A plasma-atomized powder by LPW Technology™ with 15 - 45 µm size range was utilized. The AM workpiece was manufactured using island scanning strategy with 4 × 4 mm^2 grids and subsequent layers rotations of 30°. The laser beam had a power of 105 W and a spot size of 30 µm, with a scanning speed of 950 mm/s. The layer thickness and the hatch spacing were 20 µm and 80 µm, correspondingly. The process parameters just reported, ensured obtaining a fully dense part. The conventionally manufactured workpiece was obtained from a Ti6Al4V grade 5 annealed wrought bar. Both the AM and WR workpieces were 20 × 30 × 27 mm^3 blocks with a 45° inclined surface as shown in Fig. 1.

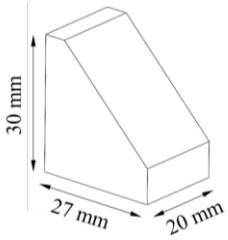

Fig. 1. Workpiece geometry.

Prior to machining, the AM pieces were heat treated to stabilize the microstructure and reduce the solidification defects [11]. The specimens were heated up at 950°C in a shielding argon atmosphere inside an RHF Carbolite Gero™ furnace for 30 min, followed by furnace cooling.

AM and WR Ti6Al4V samples for metallographic observations were prepared by grinding and polishing after hot mounting. For the final polishing a 1:4 mix of colloidal silica suspension and hydrogen peroxide 30 % was used on a polyester cloth. After 15 s of etching with the Kroll's reagent, the samples were cleansed with warm tap water and immediately dried with air blast. The microstructure was inspected with a high definition digital camera of the Leica™ DMRE optical microscope. The Vickers microhardness was obtained by a Leitz™ Durimet microhardness tester with a load of 100 gf for 15 s dwelling time according to the ASTM E92-17 standard.

2.2. Machining tests

The machining tests were carried out on a high precision machining center Kugler Micromaster® 5X with aerostatic spindle speed up to 60˙000 rpm and a vertical axis run-out less than 2 µm. The tools used for the experiments were 2 mm diameter ball nose end mills with two cutting edges made of uncoated tungsten carbide (R216.42-02030-AK60A H10F by Sandvik™ Coromant). Before executing the finishing slots, a roughing operation was carried out with two passes of 0.073 mm for both axial and radial depths of cut. Horizontal upward tool path was utilized for finishing ball end milling on 4 × 4 mm^2 slots in down cutting conditions as illustrated in Fig. 2. Each slot was milled with one set of parameters reported in Table 1, chosen among the tool supplier's datasheet. Please note that the cutting speed was selected in relation to the tool radius and not to the radius contact point with the workpiece. The feed per tooth and the cutting speed were set to 0.015 mm and 100 m/min, respectively. All the machining tests were carried out under Minimum Quantity Lubrication (MQL) conditions using the vegetable-based oil Accu-Lube™ LB 5000 lubricant at a rate of 150 ml/h. Each set of experiments was executed three times on both the AM and WR workpieces.

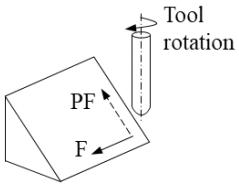

Fig. 2. Horizontal upward cutter path orientation and tool rotation. F and PF stands for Feed and Pick Feed directions, respectively.

Table 1. Cutting parameters.

ID	Cutting speed (*m/min*)	Feed (*mm*)	Axial and radial depth of cut (*mm*)
f3-d15	100	0.03	0.015
f4-d15		0.04	
f3-d73		0.03	0.073
f4-d73		0.04	

2.3. Machined surface analysis

The machined surface micro-morphology was analyzed using the FEI™ QUANTA 450 Scanning Electron Microscope (SEM). The milled surface topography was captured using the Sensofar™ PLU-Neox optical profiler equipped with a 20× Nikon™ confocal objective (0.45 of numerical aperture). For each surface, five scans of 1.5 × 1.2 mm^2 were acquired: one at the center of the machined slot and four scans at the corners. The most relevant areal surface parameters to characterize a machined surface were analyzed and processed as defined in ISO 25178 standards, and the average values reported with the relative standard deviation. The parameters taken into consideration were the amplitude parameters *Sa* (arithmetical mean height), *Sku* (kurtosis), *Ssk* (skewness), and the functional parameters *Spk* (reduced peak height), and *Svk* (reduced dale height). *Sa* parameter is commonly utilized to evaluate the

surface roughness. *Sku* is useful to indicate the prevailing of either peak or valley outliers on a surface. A surface with a normal height distribution has a kurtosis value of three, whereas a spiky surface will have higher *Sku*, and a bumpy surface lower *Sku*. The *Ssk* parameter is a measure of the surface skewness indicating the symmetry and deviation from an ideal normal distribution, for which the skewness is zero. A positive *Ssk* value indicates a majority of peaks on a surface, whereas a negative *Ssk* value designates a predominance of valleys. *Spk* represents the measure of the peak height above the core roughness of the surface, while *Svk* represents the valley depth below the core roughness.

2.4. Chip analysis

Investigation of the chip morphology and major features was conducted to assess the influence of different cutting parameters and microstructural characteristics. The chips were collected at each machining trial and observed at the SEM. The chip lamellae width, the maximum chip width, and the chip length were measured using ImageJ™. The average values of the chip features and the standard deviation were calculated for ten chips for each cutting condition.

3. Results and discussion

3.1. Microstructure

In Fig. 3 the microstructures along the height of the heat-treated AM and WR workpieces are reported. Both the alloys present α and β phases, in light and dark respectively in the images. However, evident differences between the two microstructures can be noted. The microstructure of the AM alloy is composed of α plates grouped into colonies inclined about + 45° and - 45° with respect to the Build-up Direction (BD). The α colonies lie within elongated prior β grains that developed along the BD, whereas coarse α-layers lie along the grain boundaries of the prior β grains (see Fig. 3a). These features make clear that an evident anisotropy characterizes the AM microstructure. On the other hand, the WR alloy is characterized by fine α phase equiaxed grains with β phase at the boundaries. The Vickers microhardness $HV_{0.1}$ of the two alloys resulted to be comparable, being 319 ± 20 and 317 ± 20 for the AM and WR samples, respectively. Moreover, no variations in microhardness were found among different cross sections of the AM alloy.

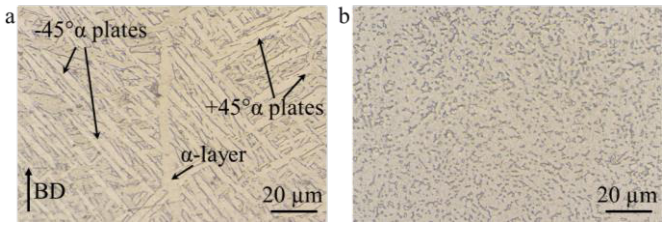

Fig. 3. Microstructure of the heat-treated AM (a), and WR Ti6Al4V alloy (b).

3.2. Surface topography

Comparing the areal roughness parameters reported in Table 2, it is possible to observe that the surface roughness *Sa* increased at least three times when machining with the higher depth of cut, at a given feed. Moreover, the roughness *Sa* slightly increased at increasing feed. These observations are in accordance to common knowledge about metal machining [12]. Nevertheless, the most interesting outcome to highlight is that the AM and WR workpieces reported dissimilar *Sa* values when machining with the higher depth of cut. In fact, machining with f3-d15 and f4-d15 cutting parameters led to comparable surface roughness values between AM and WR, whilst machining with the f3-d73 and f4-d73 put the differences among the two into light. In the latter cases, the WR machined surfaces showed 80% and 42% higher *Sa* values than the AM ones when adopting 0.03 and 0.04 mm of feed, respectively. A similar trend was noticed also for the *Spk* and *Svk* parameters. In particular, the WR surfaces machined with the higher depth of cut showed higher peaks height and deeper valleys than the corresponding AM surfaces. This is because the WR samples were characterized by more prominent feed marks. The analyzed surfaces always reported positive averaged values of *Ssk*, indicating surfaces with a predominance of spikes that protrude above the mean line. This is typical for conventional cutting operations such as milling and turning, which produce cusp-shaped topography [12]. The only exceptions were observed for the AM samples machined with f3-d15 and f4-d15, reporting negative *Ssk* values, which is peculiar of good finishing processes [12]. The samples with the highest skewness values were the WR and AM ones machined with parameters f3-d15 and f3-d73, respectively. This is related to the presence of very high peaks on the surface, such as pointy adhered particles. This was confirmed by the trend of the *Sku* values, which, in general, were higher than three denoting a spiky surface, and they were much greater for the samples just mentioned.

Table 2. Surface roughness parameters of the machined surfaces, the standard deviation is reported in brackets.

Sample	*Sa* (µm)	*Sku* (-)	*Ssk* (-)	*Spk* (µm)	*Svk* (µm)
AM f3-d15	0.17 (0.01)	5.23 (1.44)	-0.06 (0.09)	0.19 (0.01)	0.24 (0.02)
WR f3-d15	0.17 (0.01)	14.70 (4.90)	1.55 (0.37)	0.31 (0.03)	0.17 (0.02)
AM f4-d15	0.28 (0.02)	3.62 (0.30)	-0.42 (0.15)	0.24 (0.02)	0.43 (0.07)
WR f4-d15	0.25 (0.03)	5.50 (2.35)	0.06 (0.44)	0.25 (0.04)	0.40 (0.08)
AM f3-d73	0.63 (0.01)	13.93 (2.81)	1.63 (0.23)	1.24 (0.10)	0.75 (0.02)
WR f3-d73	1.16 (0.04)	6.43 (2.02)	0.48 (0.41)	1.73 (0.35)	1.37 (0.16)
AM f4-d73	0.88 (0.04)	6.51 (2.86)	0.20 (0.41)	1.20 (0.34)	1.19 (0.22)
WR f4-d73	1.24 (0.08)	6.79 (3.15)	0.69 (0.37)	1.89 (0.20)	1.32 (0.17)

3.3. Surface defects

The observations made on the areal roughness parameters were confirmed by the SEM analysis of the machined surfaces (see images in Fig. 4). It was possible to note machining feed marks in all the analyzed cases. The feed marks were denser for surfaces machined with the lower cutting depth (d15), and

were more pronounced in the case of WR samples, especially when machined at the higher cutting depth (d73). In general, the surfaces machined with the higher depth of cut reported a higher quantity of adhered material. In particular, the WR surfaces machined with f3-d73 and f4-d73 were characterized by a higher amount of large particles of adhered material, identified as smeared chips. This explains the higher *Sa* and *Spk* values found for these surfaces, as well as the *Ssk* and *Sku* values that set in the middle, accordingly to the fact that the adhered material had a bumpy morphology. On the other hand, the AM samples machined with f3-d15 and f4-d15 displayed rare adhered particles and more regular feed marks. This well correlates with the low values of all the roughness parameters reported in the previous section, in particular with the negative values of *Ssk* and the lower values of *Sku*. The surfaces of the WR slots machined with the parameters f3-d15 as well as the ones of the AM slots machined with f3-d73 were characterized

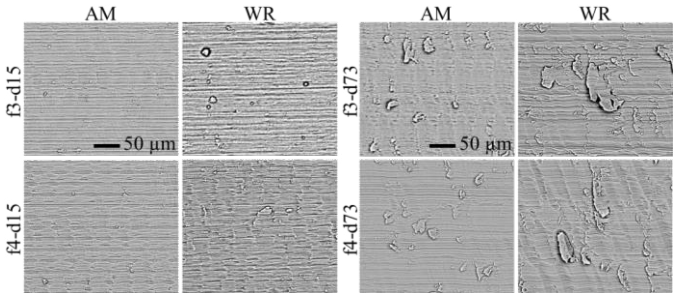

Fig. 4. Backscattered electron SEM images of the machined slots.

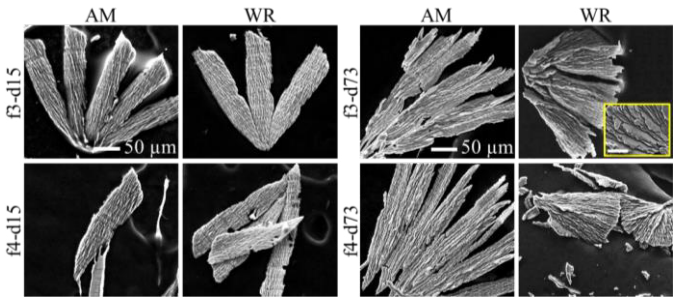

Fig. 5. Secondary electron SEM images of the chips. The yellow box shows the back surface of the WR f3-d73 sample, the relative scale bar is 50 µm

by the presence of a higher amount of small but highly prominent adhered microparticles identified as chips debris. Again, this agrees with the high values of *Ssk* and *Sku* found in these cases.

3.4. Chip morphology

Fig. 5 reports SEM images of the chips obtained under the different investigated conditions. In general, needle-like chips were obtained when machining with the lower depth of cut (d15), no matter the alloy microstructure, i.e. AM or WR. Moreover, the needle-like chips were found to be welded at one end into groups of 3-5 chips in the case of the lower feed (f3-d15). The chips welded together particularly when the higher depth of cut was adopted. In addition, serration and cracks occurred at the free ends of the chips when machining at the higher cutting depth, especially when machining the AM workpieces. The WR samples presented fan-shaped coarse chips that were highly segmented, together with elemental chips, and, in some cases, also discontinuous chips were observed. In fact, the shear planes were visible also on the back surface of the chips as showed in the yellow box in Fig. 5. Discontinuous chips are usually related to high surface roughness and irregular surface texture, confirming the observations reported in the previous sections. The development of elemental chips and metal debris is frequent in low conductivity alloys, such as Ti6Al4V, which may be due to the adiabatic shearing. The heat produced during chip forming is not dissipated fast enough and the shear becomes highly localized, causing the complete separation of the chip segments [12]. The free surface of all the chips was characterized by the presence of lamellae. The quantitative analyses reported in Fig. 6 show a linear correlation between the lamellae width and chip width at any investigated condition.

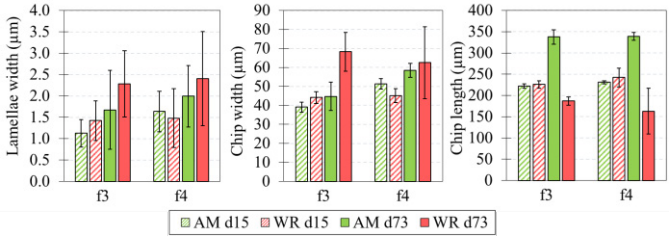

Fig. 6. Chips geometrical features.

Moreover, at the lower depth of cut (d15), AM and WR samples did not show any major difference in the chip features, other than slight differences in the chip width. The widths of the lamellae and chips slightly increased with the feed. For the higher depth of cut (d73), the widths of both the features also increased and, in general, the differences between the two alloys were more pronounced. In particular, the average values of the widths of the lamellae and chips were always higher for the WR sample. The high plastic deformation of the shear bands in the chips with wider lamellae can have contributed to the widening of the entire chips in the direction perpendicular to that of the lamellae. This can explain the similarities of the trend of the two chip features, as observed above. The chip greatest width obtained when machining WR samples with d73 may also derive from the welding of two consecutive chips along the entire chip length, because of higher friction forces developed under the most severe cutting conditions. The length of the AM chips was higher for the higher depth of cut, congruent with the fact that a greater portion of material was involved in the cutting process. The WR samples showed an opposite trend. The SEM analysis of the chips in Fig. 5 shows that the shorter length of such chips derived from the high degree of deformation of the chips in the welded ends characterized by a lumpy morphology. Furthermore, the reduction in the length of the chips can also derive from the tendency of the chips, in these cutting operations, to break into small fragments due to the adiabatic shear as previously discussed.

4. Microstructural considerations

To explain the differences observed in the machinability of the two alloys, some microstructural remarks are here reported. Recent literature studies have assessed the influence of the coarse α-layers along the BD on the machinability of the AM Ti6Al4V alloy [9]. These layers are known to act as preferential zones of severe plastic deformation [8,13], which facilitate the material removal when they are favorably aligned with the tool cutting edge during machining. Fig. 7 shows a scale model of the tool-workpiece interaction (a), and a zoom of the tool cutting edge interaction with the microstructure of the AM samples (b), at the higher cutting depth considered in this work. In Fig. 7 (b) the vertically developed α-layers are represented in dark blue, while the α plates with + 45° and – 45 ° are represented in purple and green, respectively. The effect of the vertical α-layers, is negligible in ball end milling, since their orientation is irrelevant with respect to the cutting edge that is removing the material.

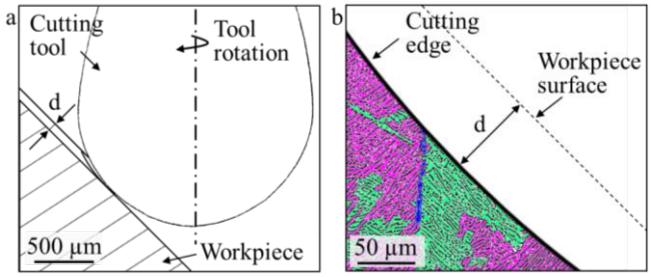

Fig. 7. Scale model of the tool-workpiece interaction (a), and zoom of the tool cutting edge interaction with the microstructure of the AM samples in case of axial depth of cut d equal to 0.073 mm (b). The α grains with different orientations are distinctly colored.

The results reported in this work showed that, at high value of depth of cut, the WR samples were characterized by higher surface roughness *Sa* than the AM ones, together with more prominent feed marks (thus higher *Spk* and *Svk*), and higher amount of adhered material. Moreover, the WR chips were more irregular, presenting welding zones, serration, or discontinuous morphology, with greater lamellae width. All these features are usually ascribed to high tool-chip friction may have been involved during the cutting process causing either surface quality deterioration [14–16], or chip irregularities [17–19]. Since no tool wear was observed at SEM after machining, and both chatter and inaccuracies in machine-tool movement were negligible, the detected differences are attributable solely to the different microstructures of the two workpieces, which induce a different material response to cutting, generating different tool-workpiece interactions. Observing the scheme reported in Fig. 7 (b), it is possible to see that in the AM sample the cutting edge may occasionally come into contact with α plates colonies with tangential orientation, which in the figure are the one colored in green. The groups of α grains tangent to the cutting edge can locally reduce the force necessary to remove the material for two reasons, namely i) the α phase is more prone to accommodate the plastic deformation than the β phase, and ii) the β phase boundaries do not hinder the plastic deformation. In fact, the β phase at the α grain boundaries is known to limit the slip length. Simultaneously, the α colonies are known to be preferential areas for the dislocations movement and crack initiation [13,20]. Therefore, as the cutting edge removes differently oriented α plates colonies, the material resistance to cutting lowers, as are the tool-chip friction, when the α colonies are tangential to the cutting edge. These microstructural features are not present in the WR samples, which were characterized by equiaxed isotropic grains, as shown in Fig. 3. Therefore, when machining WR samples, no microstructural feature allowed for a reduction of the material resistance to cutting, which thus led to the above-mentioned results. The described mechanisms have a much less effect when the smaller depth of cut is utilized, inducing the AM and WR alloys to behave approximately the same. In fact, given the same cutting conditions, the smaller the depth of cut the lower the cutting forces [21]. Therefore, the impact of differently oriented α colonies on the material resistance to cutting is less. On the other hand, when a larger portion of material is machined, the cutting forces are higher and the effect of the different microstructures can play a major role.

5. Conclusions

In this paper, the machinability of AM and WR Ti6Al4V 45° inclined workpieces was assessed in terms of surface topography, surface defects and chip morphology in case of horizontal ball end milling performed with different cutting parameters. The main findings are the following:

- The two AM and WR alloys showed an evident different machinability only when the higher depth of cut was adopted.
- The AM samples were characterized by lower quantity of adhered material with respect to the WR ones, especially at the higher depth of cut.
- The chip analysis showed irregular morphology and highly deformed shear fronts of the WR chips obtained machining with the higher depth of cut, which well correlates with the surface quality of the WR samples.
- The better machinability shown by the AM samples is ascribed to their microstructural features, namely α phase colonies tangential to the cutting edge, which may favor the material removal by locally lowering the material resistance to deformation.

Further investigations in terms of different cutting paths and workpiece inclinations are planned for a thorough comprehension of the phenomena taking place under ball end milling carried out on AM alloys anisotropic microstructure.

References

[1] Veiga C, Davim JP, Loureiro AJR. Review on machinability of titanium alloys: The process perspective. Rev Adv Mater Sci 2013;34:148–64.
[2] Leary M. Surface roughness optimisation for selective laser melting (SLM): Accommodating relevant and irrelevant surfaces. In: Brandt M, editor. Laser Addit. Manuf. Materials, Woodhead Publishing; 2017, p. 99–118.
[3] Mhamdi M-B, Boujelbene M, Bayraktar E, Zghal A. Surface Integrity of Titanium Alloy Ti-6Al-4V in Ball end Milling. Phys Procedia 2012;25:355–62.

[4] Yang P, Yao C, Xie S, Zhang D, Tang DX. Effect of Tool Orientation on Surface Integrity during Ball End Milling of Titanium Alloy TC17. Procedia CIRP 2016;56:143–8.
[5] Kasim MS, Hafiz MSA, Ghani JA, Haron CHC, Izamshah R, Sundi SA, et al. Investigation of surface topology in ball nose end milling process of Inconel 718. Wear 2019;426–427:1318–26.
[6] Yin J, Peng G, Chen C, Yang J, Zhu H, Ke L, et al. Thermal behavior and grain growth orientation during selective laser melting of Ti-6Al-4V alloy. J Mater Process Technol 2018;260:57–65.
[7] Zhao X, Li S, Zhang M, Liu Y, Sercombe TB, Wang S, et al. Comparison of the microstructures and mechanical properties of Ti-6Al-4V fabricated by selective laser melting and electron beam melting. Mater Des 2016;95:21–31.
[8] Simonelli M, Tse YY, Tuck C. Effect of the build orientation on the mechanical properties and fracture modes of SLM Ti-6Al-4V. Mater Sci Eng A 2014;616:1–11.
[9] Lizzul L, Sorgato M, Bertolini R, Ghiotti A, Bruschi S. Influence of additive manufacturing-induced anisotropy on tool wear in end milling of Ti6Al4V. Tribol Int 2020;146:106200.
[10] Bai Y, Zhao C, Yang J, Hong R, Weng C, Wang H. Microstructure and machinability of selective laser melted high-strength maraging steel with heat treatment. J Mater Process Technol 2021;288:116906.
[11] Vilaro T, Colin C, Bartout JD. As-fabricated and heat-treated microstructures of the Ti-6Al-4V alloy processed by selective laser melting. Metall Mater Trans A Phys Metall Mater Sci 2011;42:3190–9.
[12] Grzesik W. Advanced Machining Processes of Metallic Materials: Theory, Modelling, and Applications. second. Elsevier; 2017.
[13] Gil FJ, Ginebra MP, Manero JM, Planell JA. Formation of a-Widmanstatten structure: effects of grain size and cooling rate on the Widmanstatten morphologies and on the mechanical properties in Ti6Al4V alloy. J Alloys Compd 2001;329:142–52.
[14] Guo P, Zou B, Huang C, Gao H. Study on microstructure, mechanical properties and machinability of efficiently additive manufactured AISI 316L stainless steel by high-power direct laser deposition. J Mater Process Technol 2017;240:12–22.
[15] Da Silva LRR, Filho AF, Costa ES, Marcucci Pico DF, Sales WF, Guesser WL, et al. Cutting Temperatures in End Milling of Compacted Graphite Irons. Procedia Manuf 2018;26:474–84.
[16] Benardos PG, Vosniakos GC. Prediction of surface roughness in CNC face milling using neural networks and Taguchi's design of experiments. Robot Comput Integr Manuf 2002;18:343–54.
[17] Niu Z, Jiao F, Cheng K. An innovative investigation on chip formation mechanisms in micro-milling using natural diamond and tungsten carbide tools. J Manuf Process 2018;31:382–94.
[18] Wang Y, Zou B, Wang J, Wu Y, Huang C. Effect of the progressive tool wear on surface topography and chip formation in micro-milling of Ti–6Al–4V using Ti(C7N3)-based cermet micro-mill. Tribol Int 2020;141:105900.
[19] Wan ZP, Zhu YE, Liu HW, Tang Y. Microstructure evolution of adiabatic shear bands and mechanisms of saw-tooth chip formation in machining Ti6Al4V. Mater Sci Eng A 2012;531:155–63.
[20] Lütjering G. Influence of processing on microstructure and mechanical properties of (α + β) titanium alloys. Mater Sci Eng A 1998;243:32–45.
[21] Yücesan G, Altintas Y. Prediction of ball end milling forces. J Manuf Sci Eng Trans ASME 1996;118:95–103.